Water Resources Research

RESEARCH ARTICLE
10.1029/2018WR023665

Key Points:
- First study to constrain StorAge Selection functions with oxygen-18 and cosmogenic radioactive isotopes tritium, sodium-22, and sulfur-35
- The travel time distribution of a subalpine stream varies with stream flow rate, as a consequence of variable storage selection
- Subsurface water storage at the Southern Sierra Critical Zone is estimated to be 3 m on average over the entire catchment

Supporting Information:
- Supporting Information S1

Correspondence to:
A. Visser,
visser3@llnl.gov

Citation:
Visser, A., Thaw, M., Deinhart, A., Bibby, R., Safeeq, M., Conklin, M., Esser, B., & Van der Velde, Y. (2019). Cosmogenic isotopes unravel the hydrochronology and water storage dynamics of the Southern Sierra Critical Zone. *Water Resources Research*, *55*, 1429–1450. https://doi.org/10.1029/2018WR023665

Received 11 JUL 2018
Accepted 21 JAN 2019
Accepted article online 29 JAN 2019
Published online 20 FEB 2019

Cosmogenic Isotopes Unravel the Hydrochronology and Water Storage Dynamics of the Southern Sierra Critical Zone

A. Visser[1], M. Thaw[1,2], A. Deinhart[1], R. Bibby[1], M. Safeeq[2,3], M. Conklin[2], B. Esser[1], and Y. Van der Velde[4]

[1]Nuclear and Chemical Sciences Division, Lawrence Livermore National Laboratory, Livermore, CA, USA, [2]Sierra Nevada Research Institute, University of California - Merced, Merced, CA, USA, [3]Pacific Southwest Research Station, United States Forest Service, Fresno, CA, USA, [4]Faculty of Science, Earth and Climate, VU University, Amsterdam, Netherlands

Abstract One of the principal questions in hydrology is how and when water leaves the critical zone storage as either stream flow or evapotranspiration. We investigated subsurface water storage and storage selection of the Southern Sierra Critical Zone Observatory (California, USA) within the age-ranked storage selection framework, constrained by a novel combination of cosmogenic radioactive and stable isotopes: tritium, sodium-22, sulfur-35, and oxygen-18. We found a significant positive correlation between tritium and stream flow rate and between sulfur-35 and stream flow rate, indicating that the age distribution of stream flow varies with stream flow rate. Storage selection functions that vary with stream flow rate are better able to reproduce tritium concentrations in stream flow than functions that are constant in time. For the Southern Sierra Critical Zone, there is a strong preference to discharge the oldest water in storage during dry conditions but only a weak preference for younger water during wet conditions. The preference of evapotranspiration for younger water, constrained by oxygen-18 in stream water, is essential to parameterize subsurface storage but needs to be confirmed by isotopic or other investigations of evapotranspiration. This is the first study to illustrate how a combination of cosmogenic radioactive isotopes reveals the hydrochronology and water storage dynamics of catchments, constrains the subsurface architecture of the critical zone, and provides insight into landscape evolution.

Plain Language Summary Watersheds store water underground in soils and weathered bedrock. How long it takes for water to flow through the subsurface to feed streams is difficult to measure but important to understand how watersheds function. We used a novel combination of isotopic tracer methods to study the mixture of water ages in Providence Creek, a stream in the southern Sierra Nevada, California (USA). We studied naturally occurring radioactive isotopes of hydrogen (tritium), sodium-22, and sulfur-35. The abundance of these isotopes decreases because of radioactive decay as water spends more time underground. Each of these isotopes has a distinct half-life (12.3 years, 2.6 years, and 87 days, respectively). By using this combination of isotopes we were able to tease out the mixture of water ages in the stream. This level of detail helps us understand how the subsurface "selects" water from storage to generate stream flow. We find that Providence Creek has a strong preference to remove the oldest water in storage during dry conditions but shows only a slight preference to remove younger water during wet conditions. Based on the age mixtures of stream water, we estimate that the Providence Creek watershed stores 3 m of water in the subsurface.

1. Introduction

The principal question in hydrology is how water is transferred from storage to stream flow or evapotranspiration (McDonnell, 2017). The preferential transfer of water from certain parts of the storage can be viewed as a selection process controlled by the critical zone architecture (Grant & Dietrich, 2017): the connectivity and conductivity of the subsurface under variably saturated conditions controlled by soils, weathered regolith, and fractured rock. The uptake of water from storage for evapotranspiration depends on the complex interplay between climate controlling evaporative demand and the health and structure of the vegetation, in particular the root network, and the physical subsurface (Fatichi et al., 2015).

To reduce the complexity of all hydrological processes affecting the relationship between storage and discharge, the selection question can be posed as a probability of a water parcel inside the catchment to leave the catchment as either stream flow or evapotranspiration at a certain time (Van der Velde et al., 2012). In that context, the new question becomes which property or characteristic of the water parcel is predictive of the probability to exit the catchment: its position in the landscape, for example, the distance to the stream (Seibert et al., 2009); the travel time of the water parcel within the catchment, that is, the time since the parcel entered the catchment as precipitation or snowmelt; or its chemical status (Druhan et al., 2017; H. Kim et al., 2017; Liu et al., 2013). In our study, we focus on storage selection based on water age or *hydrochronology*.

We broadly define hydrochronology as the study of water ages in the critical zone. This includes studying the residence times of water in storage (saturated or unsaturated) or the travel or transit times of fluxes (e.g., stream flow or evapotranspiration) in order to understand the functioning of the critical zone, a catchment or a groundwater body, or the transport of contaminants therein. More specifically to this paper, hydrochronology refers to the sequential contribution of past precipitation events to the water balance, in terms of both fluxes (stream flow and evapotranspiration) and volumes (storage) and how these contributions change with time. This is analogous to the more general term *chronology*: the sequential order in which past events have occurred. Hydrochronology therefore extends beyond the age distribution of a flux or storage at any point in time, by emphasizing that the age distribution is time-variable and can only be the result of the sequential order in which past precipitation and discharge events have occurred. As such, it fits neatly within the framework of the age-ranked storage selection.

The age-ranked storage selection framework (StorAge Selection or SAS; Botter et al., 2011; Harman, 2015; Van der Velde et al., 2012) is an approach to quantify the probability of a water parcel to leave a catchment and reduces catchment behavior to one or more storage selection functions. The SAS framework recognizes that both the water balance and the age budget must close and provides a coherent framework to relate the storage age distribution to the stream flow age distribution (Rinaldo et al., 2015). In this framework, the water age distribution in stream flow is a consequence of the selection from storage. In turn, the age distribution of storage is the result of the entire history of past recharge and discharge events and as such of the catchment selection history.

The question arises whether these storage selection functions are properties of the catchment that are fixed in time or depend on the wetness status of the catchment, and if so, how? The mathematical derivation of age-ranked storage selection (SAS functions) has been presented elsewhere (e.g., Rinaldo et al., 2015). The storage selection framework has been tested a number of times in a variety of settings: at Plynlimon constrained by chloride concentrations (Benettin et al., 2015; Harman, 2015), at Brundtland Burn constrained by oxygen-18 (Benettin et al., 2017), in a sloping lysimeter study constrained by periodic tracer pulses (M. Kim et al., 2016), and in a vegetated lysimeter constrained by fluorobenzoate tracers (Queloz et al., 2015). We expect that the shape of the storage selection functions (and the parameters that define them) are more directly related to characteristics of a catchment, whereas the shape of the travel time distribution depends in first order on the history of hydrological events and only in second order on catchment characteristics such as the slope and drainage network (Van der Velde et al., 2012).

One catchment characteristic that is explicitly defined in the SAS framework is the total active storage volume of water. Active storage is defined here as the water stored in the subsurface that is mobile and flows toward a stream or plant roots. This presents an opportunity to derive active storage volume from the SAS framework to inform weathering and erosion rates, independent of geophysical estimates which are important field constraints but labor intensive (Holbrook et al., 2014). Assuming a steady state system, active storage can directly be determined from an estimated steady state water flux and residence time (or age; St. Clair et al., 2015). Within the dynamic SAS framework, the active storage volume can be inferred from the discharge and evapotranspiration fluxes, the age distribution of these fluxes, and assuming a selection preference from storage. It is therefore expected that evaluating catchment storage selection also informs us which parts of the catchment subsurface contribute most to stream discharge and thus on weathering rates (Rempe & Dietrich, 2014).

In a dynamic catchment—that is, any catchment—it is expected that the probability of any given parcel of water to exit the catchment is dependent on the condition of the catchment, expressed as amount of water storage or stream flow rate (Harman, 2015; Morgenstern et al., 2010): specifically, that high-flow conditions increase the probability of younger water to be discharged and that low-flow conditions increase the probability that older water is discharged. Early evidence that stream flow is older than recent snowmelt (Martinec, 1975) led to the "old water paradox" of rapid mobilization of old water (Kirchner, 2003) in traditional hydrograph separation studies (Jones et al., 2006). Beyond understanding the hydrology of catchments, the age of water also impacts water quality at the catchment scale (Benettin et al., 2015; Cartwright & Morgenstern, 2018; Rinaldo et al., 2015; Van der Velde et al., 2010).

Neither storage selection functions nor the age distribution of stream flow can be observed directly and thus must be derived from chemical or isotopic signatures of stream flow. Storage selection functions are conceptual tools to interpret chemical and isotopic signatures in streams and study characteristics of a catchment. In the 2-year study presented here, we applied a novel combination of cosmogenic radioactive and stable isotopes as hydrological tracers to study the hydrochronology of the Providence Creek watershed at the Southern Sierra Critical Zone Observatory (SS-CZO; Bales et al., 2017). The isotopic tracers are tritium (half-life = 12.32 years), sodium-22 (2.6 years), sulfur-35 (87 days), and oxygen-18 (stable).

The radioactive decay of cosmogenic isotopes, like sulfur-35, sodium-22, and tritium, results in a predictable evolution of activity concentration with water age from the moment of precipitation and provides direct information on water residence times. Aboveground thermonuclear tests between 1952 and 1963 have elevated tritium concentrations in historical precipitation. The origin of tritium in precipitation since the early 1990s (in the Northern Hemisphere) is natural cosmogenic production, and the interpretation of water younger than 30 years is no longer complicated by bomb pulse tritium. While analytical efforts for radioactive isotopes are more significant and natural (seasonal) variability in precipitation needs to be addressed, the radioactive decay makes the combination of tracers a powerful tool to unravel the age distribution of stream flow. More detailed information on the origin, prior applications, and analyses of these isotopes can be found in the supporting information Text S1.

Analysis of these four tracers in stream flow in a range of catchment conditions enabled us to investigate the age distribution of stream flow, the preference for discharging younger or older water from storage, and the subsurface storage of the critical zone subsurface. This is the first study to combine these cosmogenic isotopes to determine catchment hydrochronology on a scale from months to decades and to investigate storage selection in the critical zone.

This study revolved around three main research questions: (1) How does the critical zone of a subalpine watershed "select" water from storage for stream flow or evapotranspiration? (2) What is the shape of the age distribution of stream flow, and how does it vary with storage conditions? (3) What is the volume of subsurface storage of the watershed?

2. Materials and Methods

2.1. Field Site

The SS-CZO (Anderson et al., 2008) is located at 37.055 N, 119.205 W, in the southern Sierra Nevada mountains (California, USA) at an elevation of 1,800–2,100 m and 235 km inland from the Pacific Coast (Figure 1a). Providence Creek (4 km^2) drains a headwater catchment into Big Creek (~50 km^2) in the Kings River basin. Providence Creek is positioned on a tread in the stepped terrain of the Southern Sierras (Jessup et al., 2011). While the edges of a tread in the terrain (Figure 1b) delineate the northern and western boundaries of the Big Creek catchment, Providence Creek is located east of the tread edge, in an area with generally gentler slopes. We collected samples and present stream flow data from the P301 subcatchment (1 km^2). P301 is characterized by steeper slopes and deeply weathered granodiorite. Three meadows have formed in the past, possibly under anthropogenic influences, that are undergoing erosion at present. Precipitation, snow depth, and snow water equivalent have been monitored since 2004, as well as stream flow (Safeeq & Hunsaker, 2016). A tall eddy covariance flux tower has measured evapotranspiration and carbon fluxes above the tree canopy since 2008 (Goulden et al., 2012; Goulden & Bales, 2014).

The SS-CZO has a subalpine Mediterranean climate with a mean annual air temperature of 8 °C and an annual precipitation (mean ± standard deviation) of 1,050 ± 535 mm (Safeeq & Hunsaker, 2016), over 80% of which falls during fall and winter. The elevation of the site is at the rain/snow transition, receiving

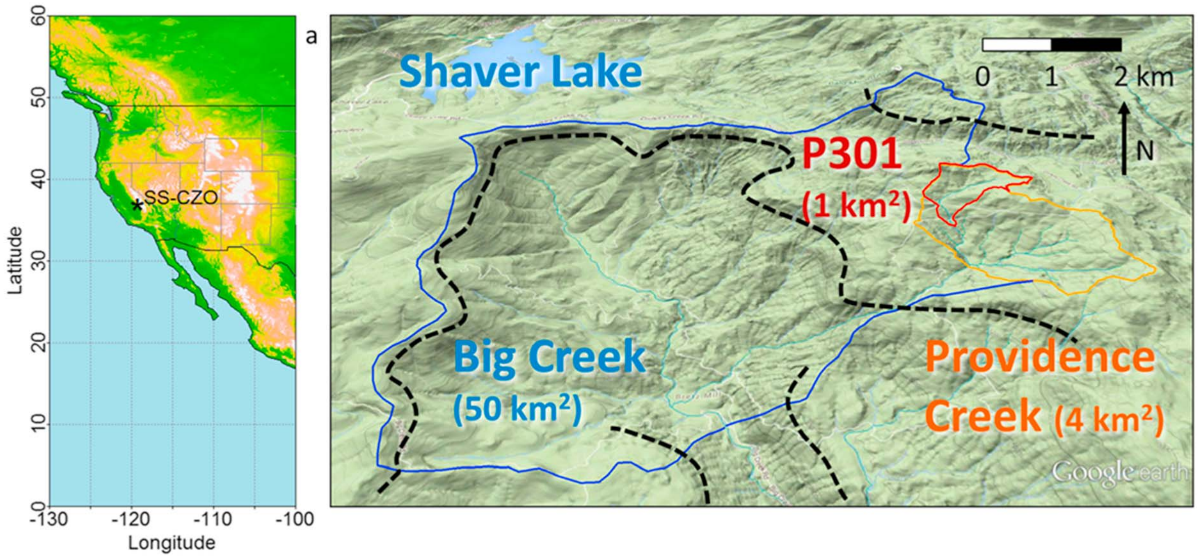

Figure 1. Location of the Southern Sierra Critical Zone Observatory (a) in California (USA) and map (b) of the P301 headwater catchment (red), Providence Creek (orange), and Big Creek (blue), near Shaver Lake, California. Dashed black lines highlight the tread edges in the stepped terrain of the southern Sierra Nevada.

approximately equal proportions of precipitations as rain or snow, but the ratio varies strongly between years. Low precipitation totals in water years (WYs) 2012 to 2015 (defined as the period between 1 October of the previous year and 30 September) resulted in a severe drought in California (He et al., 2017).

Annual stream flow varies from 22 mm during the drought in 2015 to 1,081 mm in 2011 (mean ± standard deviation = 360 ± 380 mm). Evapotranspiration removes the majority (693 ± 81 mm) of precipitation with very little interannual variability. Annual variation in precipitation is not reflected in the annual variation of evapotranspiration (11%) but instead leads to the annual variation in stream flow. The runoff ratio varies between 5% during the drought to 57% in a wet year like 2011. The Mediterranean climate leads to annual storage changes of 488 ± 244 mm, with extremes as high as 951 mm and as low as 108 mm during the drought. The analysis of the precipitation, ET, and snow depth data to calculate a long-term closing water balance is described in detail in the supporting information Text S2.

2.2. Sample Collection and Analysis

Sixteen precipitation samples were collected in WYs 2015 and 2016 to characterize levels of cosmogenic isotopes in precipitation. Twenty-five nearly monthly samples for tritium, sulfur-35, and oxygen-18 were collected from stream flow. Fewer sodium-22 samples were collected during the development of the technique. A detailed description of sample collection and analytical procedures can be found in supporting information Text S3. Reconstructed concentrations of tritium in precipitation are based on a daily air mass trajectory analysis (Visser et al., 2018). Supporting information Text S4 provides a detailed description of the reconstruction of isotopes in precipitation.

2.3. Age-ranked Storage Selection

In this study we applied the age-ranked storage selection (SAS) approach (Harman, 2015; Rinaldo et al., 2015; Van der Velde et al., 2012, 2015) given by the integral formulation of the cumulative water-age balance (equation (1); equation (8) in Benettin & Bertuzzo, 2018). Daily precipitation and snowmelt (N) fill up an age-ranked storage $P_S(\tau < T,t)\ \Delta S(t) + \overline{S_A}$, where $P_S(\tau < T,t)$ quantifies the fraction of active storage with a residence time τ, younger than T at time t. The volume of active storage is defined through $\Delta S(t) + \overline{S_A}$, where $\overline{S_A}$ is the long-term average active storage and $\Delta S(t)$ is the storage deviation from $\overline{S_A}$ derived from the catchment water balance (supporting information Text S2) and which is a model constant. Discharge (Q) and evapotranspiration (ET) remove water from storage, and $P_Q(\tau < T,t)$ and $P_E(\tau < T,t)$ are the cumulative age distributions of both fluxes.

$$P_S(\tau<T,t)\ \Delta S(t)+\overline{S_A}\ =P_S(\tau<T-t+t_0,t_0)\ \Delta S(t_0)+\overline{S_A} + \int_{t_0}^{t}N(g)\mathrm{d}g-\int_{t_0}^{t}P_Q(\tau<T-t+g,g)Q(g)\mathrm{d}g-\int_{t_0}^{t}P_E(\tau<T-t+g,g)E(g)\mathrm{d}g \quad (1)$$

As an example, consider water that is younger than 50 days at time t 10 days after the start of the simulation at t_0 ($T=50$, $t=t_0+10$). For this selection, the combined water and age balance reads as the volume of water in active storage younger than 50 days at time t 10 days equals the storage younger than 40 days at time t_0 plus the precipitation during the past 10 days minus discharge during the past 10 days consisting of water that infiltrated less than 50 days ago minus evapotranspiration during the past 10 days of water that infiltrated less than 50 days ago.

We used a numerical Euler forward scheme that subtracts small volumes from the age-ranked storage during each time step. Each rainfall event adds a new layer to the age-ranked storage (equation (2)).

$$P_S(\tau<\Delta t,t+\Delta t)S(t+\Delta t)=N(t)\Delta t \quad (2)$$

The volume subtracted from each previous rainfall event from this age-ranked storage by discharge over a time step is given by equation (3).

$$P_S(\tau<T+2\Delta t,t+\Delta t)S(t+\Delta t)-P_S(\tau<T,t)S(t)=-(I_X(P_S(\tau<T+\Delta t,t),t)-I_X(P_S(\tau<T,t),t))Q(t)\Delta t \quad (3)$$

The time step is automatically subdivided into smaller time steps for Q and E assuring that no more water is subtracted from a past rainfall event than its current volume (($I_X(P_S(\tau<T+\Delta t,t),t)-I_X(P_S(\tau<T,t),t)) \rightarrow 0$ when $\Delta t \rightarrow 0$. Q is subtracted before E, but reversing this order did not affect the results. This approach keeps a separate water balance for each rainfall event in the past and thus tracks how much of each rainfall event is still present in storage. The advantage of this approach is that we only have to take into account days with rainfall. When the volume of a certain past rainfall event in storage gets below 0.1 mm, its volume is added to the nearest past rainfall event that still has a volume (assuring an overall mass balance), reducing the number of past rainfall events in memory.

Building on previous studies (Van der Velde et al., 2012, 2015), we used cumulative Beta probability distribution functions (I_x) defined by parameters a and b to relate the age distribution of the discharge (P_Q) and evapotranspiration (P_{ET}) flux to the age distribution of the storage (P_S; equations (2),(6), and (7)). Other functions, for example, a power function (Benettin et al., 2017; Queloz et al., 2015), have also been demonstrated successfully. This relationship is commonly referred to as "selection" (Rinaldo et al., 2015) and effectively reduces the unknown variables in equation (1) to P_S. To reduce the number of model parameters, either a or b is assumed to have a value between 0 and 1, with the other set at 1 (equations (5) and (6)). If both a and b are 1, the cumulative beta function selects water from storage with no preference ($P_Q=P_S$). If a is smaller than 1, the cumulative beta function preferentially selects younger water from storage ($P_Q<P_S$). If b is smaller than 1, the cumulative beta function preferentially selects older water from storage ($P_Q>P_S$). a_Q and b_Q were allowed to vary from a minimum a value during wet conditions (a_{Qmin} at $Q=Q_{98}$, i.e., 98th-percentile discharge) and a minimum b value during dry conditions (b_{Qmin} at $Q=Q_2$, i.e., second-percentile discharge). We chose to relate a_Q and b_Q linearly to the square root of stream flow through an intermediate variable i (equation (7)). This choice was motivated by a strong linear relationship between tritium concentration and $\sqrt{Q}$ in our catchment described in section 3.2.

$$P_Q(\tau<T,t)\sim I_x(P_S(\tau<T,t);a_Q(t),b_Q(t)) \quad (4)$$

with

$$a_Q(t)=\min(i(t),1) \quad (5)$$

$$b_Q(t)=\min(2-i(t),1) \quad (6)$$

$$i(t)=a_{Qmin}+(2-b_{Qmin}-a_{Qmin})\frac{\sqrt{Q_{98}}-\sqrt{Q}}{\sqrt{Q_{98}}-\sqrt{Q_2}} \quad (7)$$

10.1029/2018WR023665

$$P_E(\tau<T,t) \sim I_x(P_S(\tau<T,t);a_E,1) \tag{8}$$

In addition to flow-dependent storage selection functions, we also tested the model with values for a_Q or b_Q that did not vary with flow.

$$P_Q(\tau<T,t) \sim I_x(P_S(\tau<T,t);a_Q,b_Q) \tag{9}$$

Considering only radioactive decay during transport, the concentration of an isotopic tracer in stream flow can be calculated from the stream age distribution with

$$C_Q(t) = \int_0^\infty C_N(t-T)e^{-\lambda T}\frac{\mathrm{d}P_Q(\tau<T,t)}{\mathrm{d}T}\mathrm{d}T \tag{10}$$

where C_N is the isotope concentration of the precipitation and $\frac{\mathrm{d}P_Q(\tau<T,t)}{\mathrm{d}T}$ the travel time distribution of discharge, and λ the decay constant of the radioactive tracer ($\lambda = 0$ for stable isotopes).

In summary, the model has four parameters: a_{Qmin} defining the preference for young water in stream flow during wet conditions, b_{Qmin} defining the preference for old water in stream flow during dry conditions; a_{ET} defining the preference for young water in evapotranspiration, and $\overline{S_A}$ defining the time average active amount of water stored (meters).

For the 25 isotope samples collected in the 2015–2016 period, 24 were between the 2nd percentile (Q_2) and 90th percentile (Figure 2a) and one was close to the 98th percentile (Q_{98}) of stream flow. Seven samples were collected during flow conditions below the resolution of the stream gauge (at Q_2). Although the quantiles of stream flow were well represented, the second highest flow conditions were approximately half of Q_{98}. Figure 2b shows how a_Q and b_Q vary with discharge for an example with $a_{Qmin} = 0.7$ and $b_{Qmin} = 0.2$.

2.4. Parameter Combinations and Model Setup

The water balance fluxes (N, Q, and ET) and storage anomaly (ΔS) for the WYs 2004–2016 were used as input to calculate the age composition of stream flow and evapotranspiration. Daily precipitation (or snowmelt) was added to an age-ranked storage array. Daily stream flow and evapotranspiration were processed alternately in 10 substeps, each time removing at most 10% of the daily flux from storage. If ranked storage volumes were emptied, the process was repeated to remove the remainder of the flux. To spin up the model and fill the storage with water of appropriate ages, the period 2004–2013 was repeated twice, followed by the entire simulation period 2004–2016. This was sufficient to flush the age-ranked storage volume from its initial conditions. Input concentrations of cosmogenic and stable isotopes in precipitation were estimated (see supporting information Text S4) and used to calculate tracer concentrations during sample days using equation (8).

We investigated which combinations of storage selection parameters are able to reproduce the observed level and variability of cosmogenic radioactive isotopes and oxygen-18 in stream flow and further how these parameters are correlated when constrained by a single isotopic tracer or a combination of tracers. For the flow-dependent selection case the model was tested with 18,000 unique parameter combinations. Evapotranspiration was assumed to have a preference for younger water that is constant in time and does not vary with flow conditions. We tested all values for a_{ET} between 0.05 and 1.0 with increments of 0.05. All values for a_{Qmin} and b_{Qmin} between 0.1 and 1 were tested with increments of 0.1. Values for the average active storage parameter $\overline{S_A}$ between 1.0 and 5 m were tested with 0.5-m increments. For the constant selection case, the model was tested with values for a_Q or b_Q between 0.1 and 1 with increments of 0.1.

Model performance was evaluated by examining the chi-square probability of the residuals between the observed and modeled isotope concentrations, accounting for the number of parameters p and the number of measurements n in the degrees of freedom. Measurement uncertainty was 0.5 pCi/L or more for tritium and 0.2‰ for oxygen-18 and set to 2.5 times the analytical error for sulfur-35 to accommodate uncertainties in the precipitation concentrations. The chi-square probability was chosen to test the ability of the model to reproduce the level of the tracer concentrations as a result of radioactive decay. Additionally, the

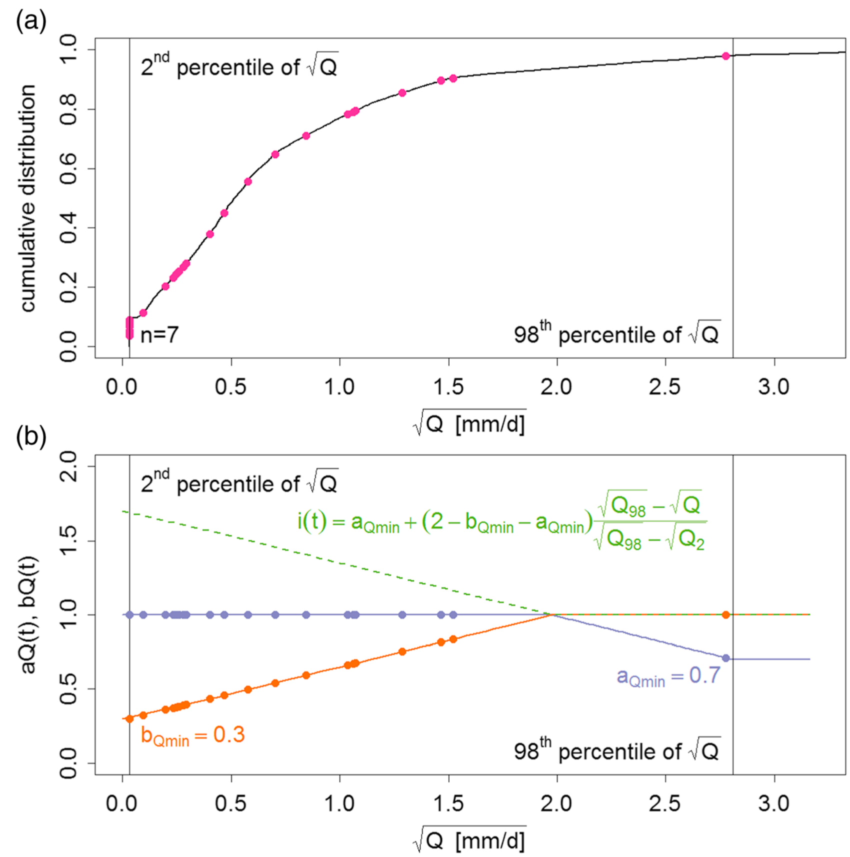

Figure 2. Cumulative distribution of square root of stream flow rate (a). Pink points indicate the stream flow conditions in which samples were collected. (b) Relation between square root of stream flow and the values of the a_Qt (blue) and b_Q(t) (orange) parameters of the beta function controlling the preference of the catchment to discharge younger water during high-flow conditions (lower $a_Q(t)$ at higher Q) or to discharge older water during low-flow conditions (lower b_Qt at lower Q).

Nash-Sutcliffe efficiency (NSE) was calculated to qualitatively evaluate model performance in terms of reproducing the variability in tracer concentrations.

3. Results

3.1. Cosmogenic, Radioactive, and Stable Isotopes in Precipitation and Providence Creek Stream Flow

During the two years of the study, Providence Creek experienced an extremely dry water year (2015) and a water year with near-average precipitation (2016; Figure 3a). The snow pack in WY 2015 was minimal and melted out in January 2015. Snow pack in WY 2016 was substantially larger and lasted through February 2016. The largest response in stream flow was to an extreme storm in early March 2016, captured in repeated sampling over a 3-day period.

Over the 2-year period, 16 precipitation samples were collected for tritium (Figure 3b). Figure S4.4 in supporting information Text S4 is scaled to include all precipitation measurements. Precipitation was collected in bins left out over a period of 1 to 84 days (33 days on average). Tritium in precipitation varied from 5.7 to 35 pCi/L, with no clear seasonal signal. The precipitation weighted mean tritium concentration in precipitation was 13.5 pCi/L.

The two long-term precipitation samples for WY 2015 and WY 2016 that were analyzed for sodium-22 both contained an activity concentration of 150 ± 30 mBq/m^3 (Figure S4.4c). In the absence of more detailed

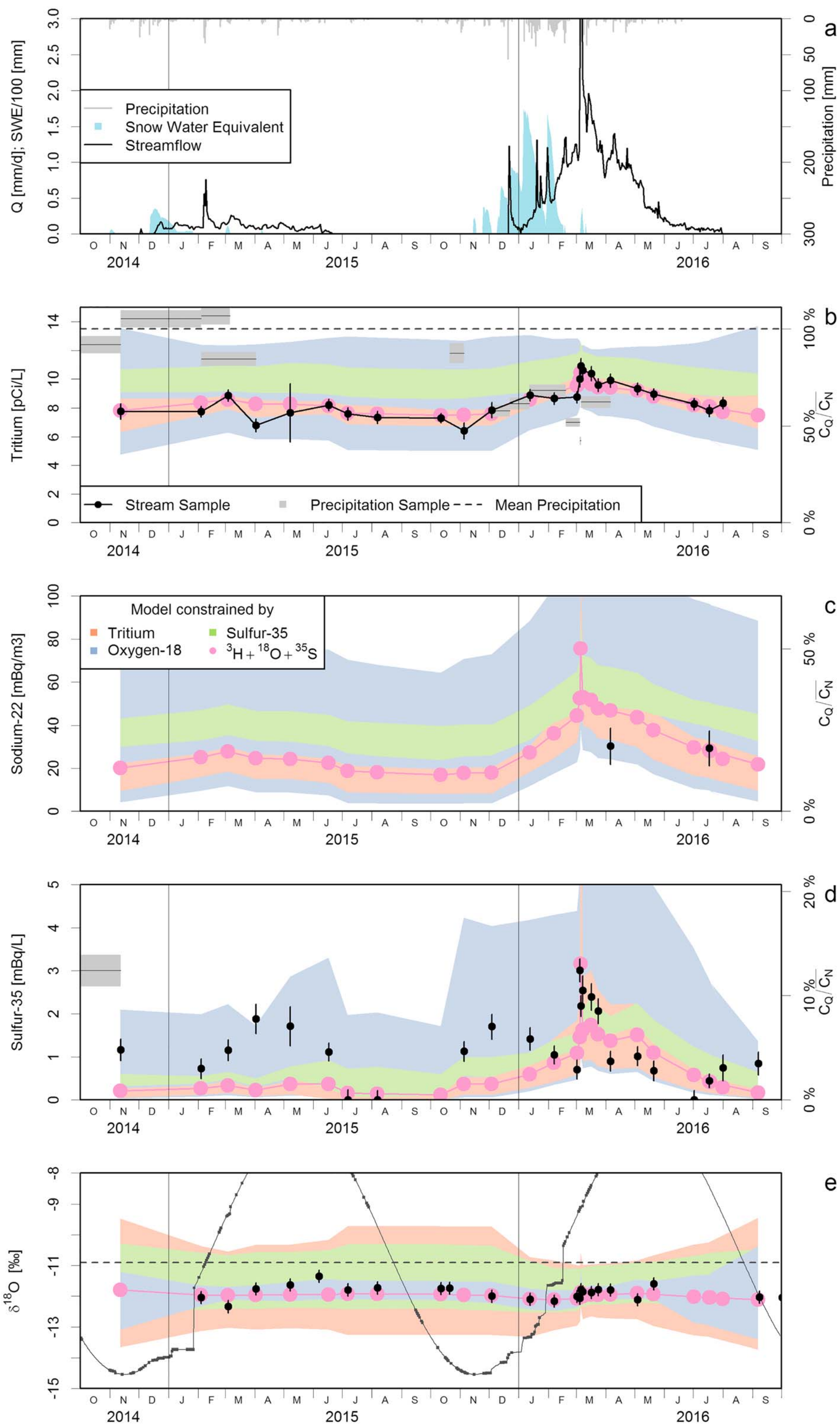

Figure 3. Time series for the Providence Creek P301 subcatchment of (a) precipitation (vertical gray bars, right axis), snow pack (blue shading), and stream flow (black line). Concentrations of cosmogenic radioactive (b–d) and stable isotopes (e). Measured isotopes in precipitation (horizontal gray bars indicating 1σ measurement uncertainty), daily input estimates (gray lines), and the precipitation weighted mean input (dashed gray line). Measured isotopes in stream flow (black symbols with 1σ measurement uncertainty). Color-shaded areas reflect isotope ranges predicted by storage selection functions, constrained by tritium (orange shading), sulfur-35 (green shading), and oxygen-18 (blue shading). Purple line and symbols are predicted by the most probable parameter combination fitted to all three isotopes. (Figure S4.4 in supporting information is scaled to include all precipitation measurements.)

information about the concentration of sodium-22 in precipitation, a constant level of 150 mBq/m^3 was assumed.

The sulfur-35 concentration in precipitation varied from 3.0 ± 0.4 mBq/L in January 2015 to 103 ± 1 mBq/L in May 2015 (Figure S4.4d). This pattern is consistent with samples collected in Martis Valley, 400 km north of the SS-CZO field site in the California Sierra Nevada. A sinusoidal function with a period of one year was assumed for sulfur-35 in precipitation, based on this data and previously collected sulfur-35 concentrations in precipitation. The precipitation weighted mean concentration of sulfur-35 in precipitation was 24 mBq/L.

Measured values of oxygen-18 (expressed as $\delta^{18}O$) in precipitation varied from −18.8‰ to 4.1‰ (Figure S4.4e). The snowmelt values were typically lower than the summer precipitation. A sinusoidal function with a period of one year approximates oxygen-18 in precipitation (Figure 3e). During snow pack accumulation, the oxygen-18 signature was delayed until snowmelt which resulted in short periods of constant oxygen-18 inputs. Here we assume that the snowmelt value is the average of all snow that is stored in the snow pack and neglect evaporation and sublimation effects. The precipitation weighted mean value for oxygen-18 in precipitation (and snowmelt) is −10.8‰.

Tritium in stream flow (Table 1) varied between 6.4 ± 0.6 pCi/L and 8.3 ± 0.4 pCi/L during low-flow conditions (10th percentile: $Q < 0.05$ mm/day). The mean tritium concentration during low-flow conditions (7.6 pCi/L) corresponds to 56% of the weighted initial concentration of tritium in precipitation (13.5 pCi/L). Tritium concentrations increased to 10.9 ± 0.5 pCi/L during high-flow conditions, corresponding to 81% of the initial concentration. These tritium concentrations correspond to a decay age ($\tau = \ln(C_N/C_Q)/\lambda$) of 4 years for high-flow conditions and 10 years for low-flow conditions, assuming a constant precipitation concentration of 13.5 pCi/L. If an exponential age distribution of stream water is assumed, the mean age ($\tau = (C_N/C_Q - 1)/\lambda$) would range from 4 to 14 years. Variations of tritium in stream flow were smaller in WY 2015 than in WY 2016, as a result of very low flow during the last year of the 2012–2015 drought in California.

Sodium-22 concentrations in stream flow (30.3 ± 8.5 and 29.3 ± 8.1 mBq/m^3) were approximately 20 ± 5% of precipitation (151 ± 9 mBq/m^3, $n = 3$). Too few samples were successfully analyzed to evaluate variability in stream flow. Sulfur-35 concentrations varied from nondetectable (<0.5 mBq/L) to 6.7 mBq/L in stream flow, corresponding to 28% of precipitation weighted initial concentrations. Unlike tritium, the sulfur-35 concentration appears to be delayed with respect to peak flow conditions. Sulfur-35 concentrations responded to higher winter stream flow in both 2015 and 2016, while tritium concentrations only responded to the flow conditions in 2016.

Oxygen-18 varied very little (−12.3‰ to −11.4‰) with stream flow conditions (Figure 3e). The low levels of cosmogenic isotopes and small variation of oxygen-18 point to an age distribution with a mean of several years, in both low and high-flow conditions. While very little variation in oxygen-18 was observed, the abundance of oxygen-18 in the stream was consistently below the precipitation weighed input signature, representing a general preference to discharge winter precipitation in stream flow.

3.2. Correlation Between Cosmogenic Isotopes and Stream Flow

Tritium concentrations were linearly correlated with the square root of stream flow rate ($R^2 = 0.75$, $p < 0.001$, Figure 4). Sulfur-35 concentrations were also linearly correlated with the square root of stream flow rate (Figure 4b), although the correlation was weaker ($R^2 = 0.37$) but still significant ($P < 0.01$). We interpret this positive linear correlation as younger water being discharged during high-flow conditions and older water during low-flow conditions. We attribute the weaker correlation for sulfur-35 to the higher sensitivity to input variability. The shorter half-life of sulfur-35 makes it particularly sensitive to the fraction of youngest water (less than 1 year old) in stream flow. The significant correlations are evidence that the age distributions of stream flow depends on the hydrological conditions of the watershed.

3.3. Modeled Isotopes in Stream Flow

Parameter combinations were first tested by comparing modeled and observed concentrations of tritium, sulfur-35, or oxygen-18 separately and secondly by including all three isotopes in the objective function. For tritium, 355 parameter combinations resulted in a residual between the observed and modeled concentrations corresponding to a chi-square probability larger than 0.05 (Pchisq > 0.05, 25 observations, 4

Table 1
Flow Rate and Isotopes of Tritium, Sodium-22, Sulfur-35, and Oxygen-18 in P301 Stream Flow

Collection date	Stream flow (mm/day)	Tritium (pCi/L)	±	Sodium-22 (mBq/m^3)	±	Sulfur-35 (mBq/L)	±	Oxygen-18 (‰)	±
11/12/2014	0.00	7.8	0.6			1.17	0.25		
2/4/2015	0.09	7.7	0.4			0.73	0.23	−12.0	0.2
3/4/2015	0.16	8.9	0.4			1.16	0.24	−12.3	0.2
4/2/2015	0.07	6.8	0.5			1.88	0.34	−11.8	0.2
5/8/2015	0.07	7.7	2.0			1.71	0.45	−11.6	0.2
6/17/2015	0.04	8.2	0.4			1.12	0.21	−11.4	0.2
7/7/2015	0.00	7.6	0.4			0.00	0.24	−11.8	0.2
8/7/2015	0.00	7.3	0.4			0.00	0.22	−11.7	0.2
10/12/2015	0.00	7.3	0.3					−11.8	0.2
11/5/2015	0.00	6.4	0.6			1.13	0.23	−11.7	0.2
12/4/2015	0.00	7.8	0.5			1.70	0.29	−12.0	0.2
1/13/2016	0.22	8.9	0.4			1.42	0.26	−12.1	0.2
2/7/2016	0.49	8.7	0.4			1.05	0.21	−12.2	0.2
3/2/2016	1.13	8.8	0.4			0.71	0.22	−12.0	0.2
3/5/2016	2.31	10.0	0.6			3.01	0.27	−12.1	0.2
3/6/2016	7.71	10.9	0.5			2.18	0.24	−11.8	0.2
3/8/2016	2.15	10.6	0.5			2.54	0.34	−11.9	0.2
3/17/2016	1.66	10.4	0.5			2.39	0.31	−11.9	0.2
3/24/2016	1.15	9.6	0.5			2.06	0.29	−11.8	0.2
4/6/2016	1.07	9.9	0.5	30	9	0.90	0.23	−11.8	0.2
5/4/2016	0.71	9.3	0.4			1.02	0.22	−12.1	0.2
5/21/2016	0.33	8.9	0.4			0.68	0.23	−11.6	0.2
7/2/2016	0.08	8.3	0.4			0.00	0.22		
7/18/2016	0.06	7.8	0.4	40	10	0.45	0.16		
8/1/2016	0.01	8.3	0.4			0.75	0.30		

Note. Dates are formatted as MM/DD/YYYY.

parameters, 21 degrees of freedom). The range of tritium concentrations predicted by these 355 combinations closely followed the observed tritium (Figures 3b–3e).

The sodium-22 concentrations predicted by these 355 parameter combinations are in the same range as the measured concentrations, but too few measurements were available to evaluate the temporal variability or the dependency on stream flow rate. The tritium-constrained parameter combinations predicted sulfur-35 concentrations in the same range as the measurements, indicating that the proportion of very young (<1 year) water in the stream was simulated correctly. The parameter combinations were not able to reproduce the sulfur-35 variability well (highest NSE = −0.04). The model predicted an increase in sulfur-35 concentrations during the 2016 snowmelt season and a spike in sulfur-35 during a storm in March 2016.

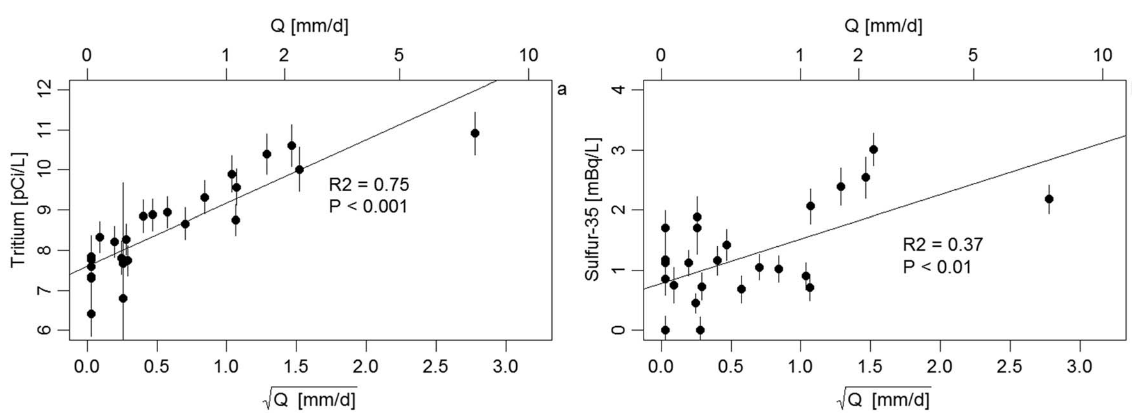

Figure 4. Tritium (a) and sulfur-35 (b) concentrations correlate significantly with the square root of stream flow *Q*.

However, the observed variations in 2015 and earlier in 2016 were not reproduced. The tritium-constrained parameter combinations predicted a wide range in delta oxygen-18 values indicating that oxygen-18 can potentially further constrain the set of probable parameter combinations.

For sulfur-35, 114 parameter combinations resulted in a probable residual between the observed and modeled concentrations (Pchisq > 0.05, 25 observations, 4 parameters, 21 degrees of freedom). These combinations predict a generally narrow range of tracer concentrations (green shading in Figures 3b–3e), often higher than the observed values for sodium-22 and tritium. The highest NSE for sulfur-35 for these 114 combinations was 0.19, indicating that they did not capture the variability of sulfur-35 concentrations well. Two reasons can cause the inability to capture the observed sulfur-35 variability. First, as noted before, sulfur-35 is more sensitive to short-term variability in input concentrations, because of the shorter half-life. Second, sulfur-35 concentrations are only very sensitive to a small part of the overall SAS function, namely, the younger water. Although the beta function seems to be a good first-order approximation for the entire storage, the SAS function can have any shape as a result of the critical zone architecture and is not likely to be as smooth as a beta function. Effects that cannot be captured by a Beta distribution are especially visible for a short-lived tracer that only depends on a small range of the entire Beta distribution.

For oxygen-18, 1,127 parameter combinations resulted in a probable residual between the observed and modeled values (Pchisq > 0.05, 19 observations, 4 parameters, 15 degrees of freedom). The highest NSE for oxygen-18 achieved by these 1,127 parameter combinations was 0.31 (compared to a NSE of 0.82 for tritium in the same set), highlighting that the average oxygen-18 abundance was better reproduced (and in this case more valuable) than the variability of oxygen-18, which was almost absent. These parameter combinations resulted in a wider range of predicted tritium, sodium-22, and sulfur-35 concentrations, which all include the range of the measured isotopes (Figures 3b–3d, blue shading).

Combining tritium, sulfur-35, and oxygen-18 in the chi-square objective function, only two parameter combinations yielded probable residuals (Pchisq > 0.05, $n = 71$, $p = 4$, 67 degrees of freedom). The parameter combination with the highest overall chi-square probability (0.06) had a NSE of 0.78 for tritium, 0.09 for oxygen-18, and −0.09 for sulfur-35 (Table 2). The parameters in this combination were an average water storage parameter $\overline{S_A}$ of 3 m, a weak preference for young water in stream flow during wet conditions ($a_{Qmin} = 0.7$), a strong preference for old water in stream flow during dry conditions ($b_{Qmin} = 0.3$), and a strong preference for young water in evapotranspiration ($a_{ET} = 0.25$). The parameters for the second best combination were similar ($\overline{S_A} = 3$ m, $a_{Qmin} = 0.7$, $b_{Qmin} = 0.2$, $a_{ET} = 0.3$,).

3.4. Probable Parameter Combinations

To evaluate the sensitivity of the fractional SAS parameters to the isotopic constraints, we studied the correlations between parameter values in the probable combinations. Combinations of a_{Qmin}, b_{Qmin}, a_{ET}, and $\overline{S_A}$ that reproduced the measurements of a single tracer vary across a wide range of values (Figure 5). The tritium time series did not constrain the preference for younger water during wet conditions (a_{Qmin}) well, possibly due to the limited number of samples collected in high-flow conditions. On the contrary, within the 355 probable combinations, b_{Qmin} is well constrained between 0.2 ($n = 139$) and 0.3 ($n = 156$). This means that the observed tritium concentrations indicate a strong preference of the catchment to discharge the oldest water in storage during dry conditions.

There is correlation between parameters a_{ET} and $\overline{S_A}$ (Figure 5c). A larger value for $\overline{S_A}$ is compensated by a larger value for a_{ET}, representing less preference for the youngest water for evapotranspiration, when constrained by tritium alone. Less preference for the youngest water results in older water leaving the catchment as evapotranspiration, effectively removing accumulated age to compensate for the older ages in a larger storage. The result is that the age of the discharge remains similar, as constrained by tritium. Whether values for a_{ET} close to 1 are realistic—that is, whether vegetation can access water of all ages in storage equally—is not constrained by the stream flow tritium data alone. Large values for the a_{ET} parameter in combination with large values of $\overline{S_A}$ also result in an oxygen-18 signature of evapotranspiration that is close to the annual mean. A stronger preference for younger water ($a_{ET} \ll 1$) shifts oxygen-18 in evapotranspiration toward summer precipitation (which is youngest when ET is highest), and consequently shifts oxygen-18 in stream flow toward winter precipitation. All oxygen-18 measurements were well below the mean weighted precipitation input (Figure 3e).

Table 2
Parameter Values and Performance Metrics of the Parameter Combination With the Highest Combined Chi-Square Probability

Parameters				Tritium			Oxygen-18			Sulfur-35			All
$\overline{S_A}$	a_{Qmin}	b_{Qmin}	a_{ET}	NSE	Chi^2	P	NSE	Chi^2	P	NSE	Chi^2	P	P
3.0	0.7	0.3	0.25	0.78	26.6	0.18	0.09	15.9	0.39	−0.09	41.1	0.005	0.06

Note. NSE = Nash-Sutcliffe efficiency.

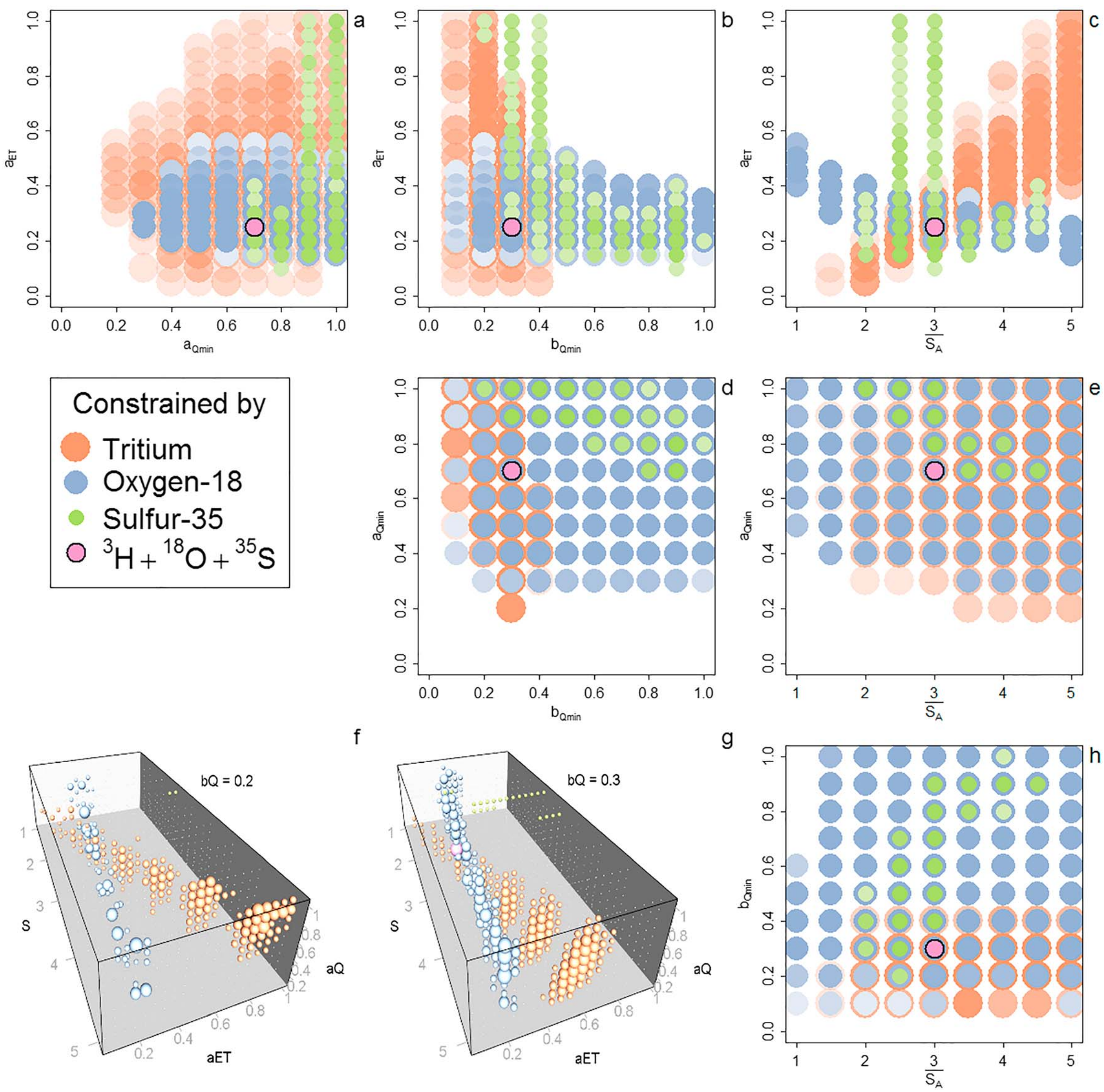

Figure 5. Correlations between parameters (a–e, h) of probable (Pchisq > 0.05) combinations, constrained by a single tracer: tritium (orange shading, outer circle), oxygen-18 (blue shading, middle circle), or sulfur-35 (green shading, inner circle). Shading intensity reflects the number of combinations with a chi-square probability of 0.05 or greater. The black circled purple dot locates the parameter combination with the highest chi-square probability, constrained by all three tracers. Three-dimensional representation of probable parameter combinations (with a chi-square probability of 0.05 or greater) constrained by tritium (orange) or oxygen-18 (blue) or sulfur-35 (green), with b_{Qmin} fixed at 0.2 (f) or 0.3 (g). The purple dot (in g) represents the parameter combination with the highest chi-square probability, constrained by all three tracers. Parameter combinations with a higher probability are represented by larger spheres. A correlation between a_{ET} and a_{Qmin} at high values for $\overline{S_A}$ and $b_{Qmin} = 0.3$ is visible (in g) that was not apparent from the two-dimensional parameter correlation figures.

10.1029/2018WR023665

Parameter sets constrained by oxygen-18 only (Figure 5, blue dots, intensity representing number of probable combinations) show an opposite correlation. A larger average storage parameter $\overline{S_A}$ is associated with a stronger preference for younger water in ET (smaller b_{Qmin}), to maintain a similar bias for winter precipitation. While b_{Qmin} is well constrained by tritium, a_{ET} is better constrained by oxygen-18.

Parameter sets constrained by sulfur-35 only (Figure 5, green dots) cover a wide range of values for a_{ET} (0.2–1.0) and b_{Qmin} (0.2–1.0) and also include larger values for $\overline{S_A}$. Higher values for b_{Qmin} accommodate younger water during low-flow conditions and as a result higher concentrations of sulfur-35. Parameter combinations constrained by sufur-35 show highly nonlinear correlation patterns.

Figure 5 shows that isotopic tracers separately allow for a wide range of acceptable and highly correlated parameter combinations. Only the combined application of different tracers constrains the acceptable parameters to a limited range. This is particularly well illustrated for the combination of a_{ET} and $\overline{S_A}$ (Figure 5c) where the best combination lies at the intersection of the fields of highly correlated parameters.

3.5. Constant Versus Flow-Dependent Storage Selection

The lowest chi-square residual between predicted and measured tritium of any of the constant-in-time parameter combinations was 87, with $a_Q = 1$, $b_Q = 0.4$, $\overline{S_A} = 1$, and $a_{ET} = 0.5$. The chi-square value corresponds to a probability of 10^{-9}, considering 25 measurements and 3 parameters (22 degrees of freedom). The highest NSE with a constant selection was 0.28 (for $a_Q = 1$, $b_Q = 0.6$, $\overline{S_A} = 2$, and $a_{ET} = 0.3$). The low probability of the best parameter combination, compared to higher probabilities for the variable selection functions, agrees with the notion that the observed variability in tracers in stream water is the result of the behavior of the catchment to preferentially discharge younger water from storage during wet conditions and older water during dry conditions.

3.6. Probable Storage Selection Functions

Figure 6 shows the range of shapes for the probable parameter combinations constrained by tritium, oxygen-18, and sulfur-35 or all three tracers and the optimal parameter set. During high-flow conditions, the catchment showed a mild preference to discharge the younger water in the storage as stream flow. Sulfur-35 is the strongest constraint on this parameter, while tritium and oxygen-18 both allow for a wide range of preferences. During dry conditions the catchment has a strong preference for the oldest water in storage. The preference is mostly constrained by tritium, while oxygen-18 and sulfur-35 allow for a wide range of preferences. The preference function for evapotranspiration is very well constrained by the combination of all three tracers, while each of the tracers alone allow for a wider range of preference functions.

3.7. Age Distributions in Storage, Stream Flow, and Evapotranspiration

We investigated how the shape of the age distribution of storage, stream flow, and evapotranspiration compare to exponential model (EM) age distributions and how these varied in time with hydrological conditions in the catchment. Flow-weighted cumulative age distributions for stream flow, evapotranspiration (averages of daily age distributions weighted by daily fluxes), and storage for each of the 13 years in the modeled period have a large interannual variability and reflect the seasonal Mediterranean climate. The shapes of annual average age distributions of water in storage predicted by the best parameter combination model were similar to the shape of an exponential distribution with the same mean age (Figure 7a). Differences between the modeled age distributions and an exponential age distributions were largely due to the 2012–2015 drought that followed an extremely wet year (2011). This sequence of events resulted in a gentle slope in the age distribution from 1–5 years and a steeper slope at 5–6 years. The precipitation amount in 2016 was near the long-term average, and it contributed approximately 20% to the total storage. The 2012–2015 drought resulted in a lack of recharge of younger water and an increase of the mean age in storage from 3.5 years in 2011 to 5.6 years in 2015.

Annual average age distributions of stream flow (Figure 7b, average of daily age distributions weighted by daily stream flow rate) varied strongly from year to year in response to stream flow rates and storage selection (Table 3). Stream flow exported older water in dry years (2014, 2015) than in wet years (2005, 2011). The mean age of stream flow ranged from less than 4 years (in 2005, 2006, and 2011) to more than 10 years in 2015. The 2012–2015 drought resulted in an increased age of stream flow, due to lower flows and a stronger preference for the oldest water, as well as a lack of recharge of younger water. The mean age of all stream

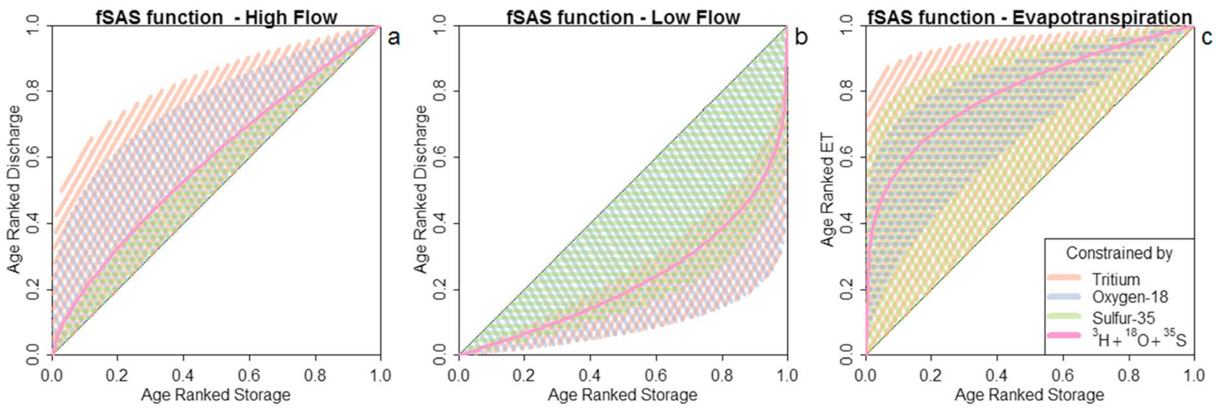

Figure 6. Fractional StorAge selection (SAS) functions for stream flow during high-flow conditions (a) and low-flow conditions (b) and for evapotranspiration (c). Shading color represents the isotope used to constrain the parameter combinations: orange = tritium, blue = oxygen-18; and green = sulfur-35. The most probable combination considering all three isotopes (purple line) shows a slight preference for younger water during high-flow conditions ($a_{Qmin} = 0.7$), a strong preference for older water during low-flow conditions ($b_{Qmin} = 0.3$), and a strong preference for younger water in evapotranspiration ($a_{ET} = 0.25$).

flow in the simulated period (2004–2016), weighted by stream flow rate, was 4.4 years, closely resembling the mean age of storage. The envelope of EM age distributions did not capture the variability in modeled age distributions, especially during drought years 2014 and 2015. In particular, the EM age distribution predicted a long tail that is absent from the modeled age distributions.

The variability in the age distribution of evapotranspiration directly reflects the age of storage because the storage selection preference for evapotranspiration was constant. The mean age of evapotranspiration was less than 2 years, except during the last years of the drought (2014 and 2015) and the following year with normal precipitation (2016). Between 44% and 72% of ET was derived from water that is less than 1 year old. The shape of the ET age distribution was not well represented by an EM, because of the strong preference for younger water.

The same variability is visible in the mean stream flow age distribution aggregated for each of the five quantiles of stream flow rate (Figure 7d). These represent the average age distributions for varying flow conditions. Daily stream flow was classified in one of five quantiles. Quantile boundaries are 0.04, 0.18, 0.40, and 1.2 mm/day. Age distributions of stream flow, evaporation, and storage were averaged for all days within the same stream flow class (quantile). During the highest quantile of flow conditions, the stream flow age distribution was slightly younger than the age distribution of water in storage.

Most water was discharged during high-flow conditions (with little preference) and by ET (with a strong preference for younger water). A preference for younger water in discharge normally leads to an age distribution in storage with a long tail. In this case, the preference for old water during low-flow conditions removed that tail from storage.

The combination of a strong preference for old water and an exponential age distribution results in a near-uniform age distribution in low-flow discharge. In this distribution, the contribution of 0–5 year old water was less than 10%. During high-flow conditions, the fraction of water in discharge less than 1 year old was still limited to 37%, consistent with the low observed concentrations of sulfur-35 and sodium-22.

4. Discussion

4.1. Transient Water Ages

We found a significant positive correlation between tritium and the square root of stream flow rate, confirming that the age distribution of stream flow varies with stream flow rate. We interpret the variation in tritium as younger water being discharged during high-flow conditions and older water during low-flow conditions and confirmed this with fractional storage selection functions. End-member mixing analysis in this catchment showed that stream flow was dominated by subsurface flow, with an average contribution greater than 60% (Liu et al., 2013). The finding that snowmelt runoff contributed less than 40% (Liu et al., 2013)

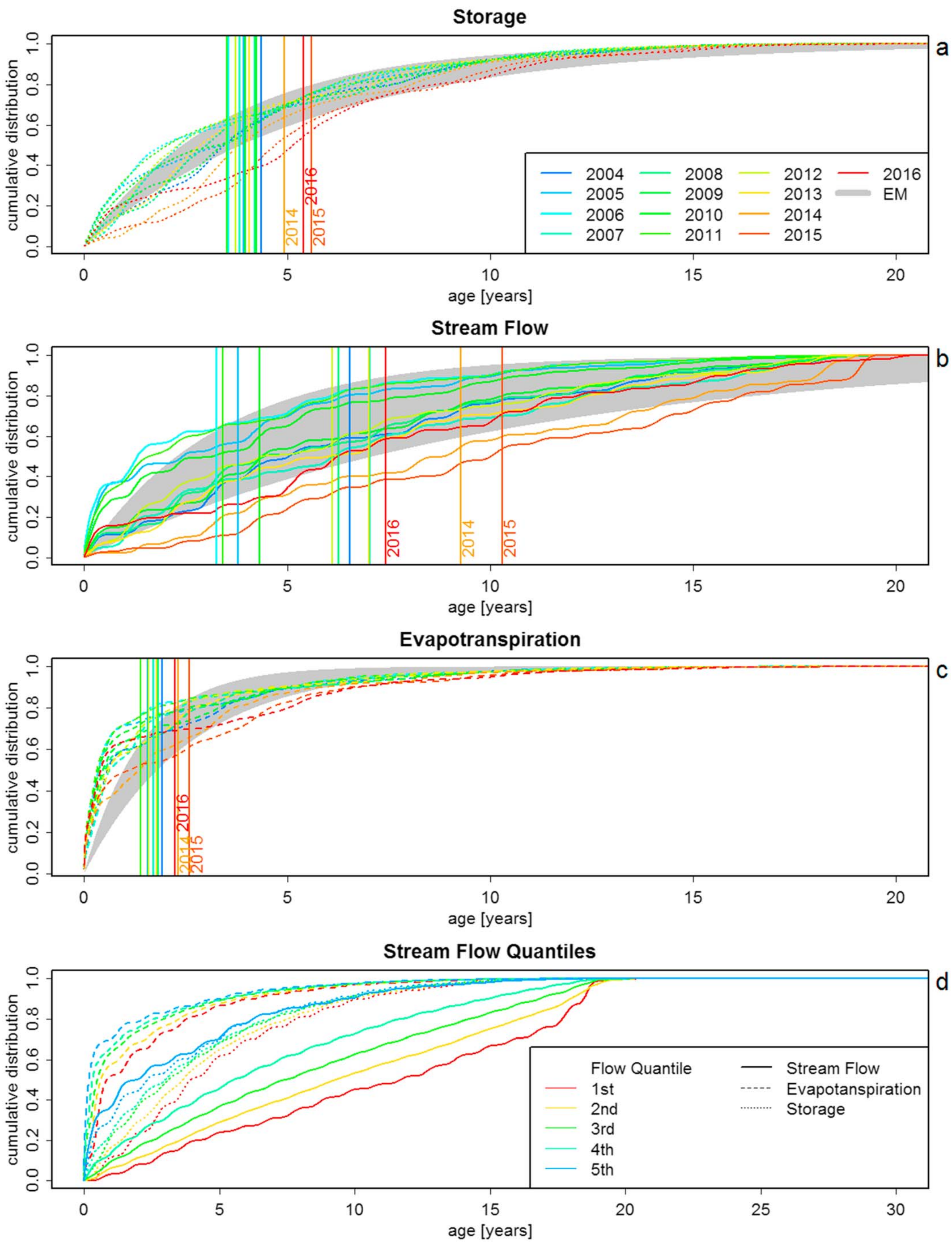

Figure 7. Flow-weighted cumulative age distributions for storage (a), stream flow (b), and evapotranspiration (c) for each of the 13 years in the modeled period showed interannual variability and the seasonal effects of the Mediterranean climate. The envelope of exponential model (EM) age distributions (gray shading) does not capture the variability in modeled age distributions, especially during drought years 2014 and 2015. Vertical lines show how the mean age of each component shifts from year to year, with years 2014 and 2015 affected by the drought. Cumulative age distributions for stream flow, evapotranspiration and storage, averaged over five quantiles of stream flow rates (d).

corresponds to the low peak sulfur-35 concentration we observed during peak flow in 2015. We found that on average, the flow-weighted percentage of water less than 1 year old in stream flow was 31%.

It is generally accepted that high-flow conditions mix event water with pre-event water. Other studies have demonstrated that travel times distribution of stream flow depends on catchment state, based on stable

Table 3
Calculated Mean Age of Stream Flow Q, Evapotranspiration ET, and Storage S (Weighted by Daily Fluxes or by Daily Storage Amount) for the Best Parameter Combination

Water year	Mean age (years)		
	Q	*ET*	*S*
2004	6.5	1.9	4.4
2005	3.8	1.6	3.9
2006	3.3	1.4	3.5
2007	7.0	1.7	3.8
2008	6.3	1.8	4.2
2009	6.1	1.8	4.2
2010	4.3	1.6	4.0
2011	3.4	1.4	3.5
2012	6.1	1.6	3.7
2013	7.0	1.8	4.1
2014	9.3	2.3	4.9
2015	10.3	2.6	5.6
2016	7.4	2.2	5.4
all	4.4	1.8	4.2

isotopes of water (McGuire & McDonnell, 2006) or chloride and nitrate concentrations (Van der Velde et al., 2010). We show here that event water represents only a small fraction of high-flow discharge and the change in the age distribution can be attributed to a changing preference for younger water. We also find that storage selection functions that vary with stream flow rate are significantly better able to reproduce tritium concentration in stream flow than SAS functions that are constant in time, considering the number of parameters used. This confirms that the correlation between tritium and stream flow is due to changing selection of water from storage, rather than a fixed selection of a changing composition of water ages in storage.

While the SAS framework is able to reproduce the major characteristics of the cosmogenic tracer concentrations in stream flow, it does not capture the variability in sulfur-35 concentrations well. Specifically, it does not reproduce the higher concentrations in stream flow in the spring and fall of 2015, indicating that the selection function does not capture fast flow paths adequately during these conditions. It is possible that the meadows within the catchment (<5% of the surface area) generated the runoff with young water in 2015. Meadows respond differently to precipitation inputs as upward seepage sustains high groundwater levels year-round and reduces the storage potential. The catchment as a whole reacts much stronger to the winter after the drought in 2016. For this study we treated the catchment as a whole and we did not include contrasting rainfall-runoff responses for various parts of the catchment. Therefore, it cannot be expected that a single storage selection function is accurate for such a small fraction of the total flow (the young water that affects sulfur-35), but we show that SAS functions are able to describe the cumulative age contributions of the total flow fairly accurately. As a consequence, the model parameterization relies heavily on the level and variability of tritium and oxygen-18 in stream flow. A storage selection function that is more flexible than the Beta distribution considered here could improve the model's ability to reproduce these features, possibly at the cost of nonuniqueness in the parameterization.

A similar dependence on wetness, expressed as either stream flow rate or storage, was found in lowland catchments (Van der Velde et al., 2012), the Gårdsjön and Marshall Gulch catchments (Van der Velde et al., 2015) as well as lysimeter studies (M. Kim et al., 2016; Pangle et al., 2017; Queloz et al., 2015). Although the initial proposition of fractional StorAge Selection (fractional SAS) functions (then called STorage Outflow Probability functions) would be a catchment property (Van der Velde et al., 2012), we must further explore how the catchment preference changes with wetness to find meaningful links with physical and biological catchment characteristics. This calls for a consistent evaluation of fractional SAS and other SAS models in catchments across climatic, ecological, and geological transects.

We found that the storage selection functions that best reproduce the tracer data result in a near-exponential distribution of water ages in storage. The old tail of the age distribution in storage is removed by the preference for old water during low-flow conditions. The high stream flow and evapotranspiration age distributions are skewed toward younger water. In contrast, the age distribution of base flow is nearly uniform, with a small contribution of younger water, due to the lack of water between 1 and 5 years old as the result of a drought. A similar feature was present in a SAS evaluation of a lysimeter study, with a pronounced absence of the youngest water related to unsaturated zone storage (Queloz et al., 2015).

In our work, we related a_{Qmin} and b_{Qmin} of the beta distribution (describing catchment preference) to the square root of the stream flow rate, based on preliminary results. Alternatively, the a_{Qmin} and b_{Qmin} of the beta distribution can be related to storage or the logarithm of stream flow rate, or another indicator of catchment wetness. Instead of varying either a_{Qmin} and b_{Qmin} between 0 and 1, both parameters could be allowed to vary simultaneously, if sufficient data are available to constrain all parameters. Other formulations of the catchment preference function are also possible. The ranked StorAge Selection (rSAS) formulation, relating preference to absolute age-ranked storage rather than fractional (scaled) age-ranked storage, could result in a slightly different interpretation of the behavior of catchments like the SS-CZO because the seasonal variation in storage significantly rescales the fractional age-ranked storage (Harman, 2015).

4.2. Age Tracers

Tritium has often been used to study the mean age of stream flow under steady state assumptions. A study of tritium in a larger (95 km^2) catchment incorporating headwater catchments and an alluvial plain in a humid subtropical climate in Australia (Duvert et al., 2016) found no significant correlation between stream flow and tritium ($r = 0.47$, $t = 0.06$). The tritium time series were instead interpreted using a series of lumped parameter models and were considered to be beneficial in determining both the age and fraction of a contribution of old water from the flood plain to stream flow. Correlations between tritium and stream flow, supported by chemical analyses, have been explained by mixing between young recent recharge and older water stored in the catchment (Hofmann et al., 2018). A decrease in tritium concentrations was observed in the majority of the Sierra Nevada rivers from summer/fall 2013 to winter/spring 2013/2014 (Harms et al., 2016) and attributed to a greater proportion of low-tritium groundwater contribution to surface waters in 2013–2014 winter/spring samples collected in drought conditions. Tritium concentrations in French rivers not impacted by nuclear facilities were twice lower than reconstructed concentrations in precipitation. Observed variability in rivers was explained by tritium variability in precipitation, watershed area, and altitude, but not by seasonality or stream flow rate (Ducros et al., 2018).

The tritium fallout from nuclear testing has long complicated interpretation of tritium concentrations in streams and required a series of tritium measurements to derive a mean age, prescribing the shape of the distribution. In catchments where the range of water ages is limited to 30 years, or the contribution of bomb-transient ages (30–70 years) minimal, we expect that correlations between tritium and stream flow will be significant due to larger contributions of younger water and a monotonous decrease of tritium with water age. This condition already exists in the Southern Hemisphere which now has a longer time period with constant tritium in precipitation.

This is the first study to evaluate three cosmogenic radioactive isotopes tritium, sodium-22, and sulfur-35 and one of the stable isotopes of water (i.e., oxygen-18) as hydrological tracers to determine the age distribution of stream flow. In this watershed, with relatively old stream flow ages, tritium concentrations alone were not sufficient to constrain all four parameters of the fSAS model. While the preference for older water during dry conditions (b_{Qmin}) was well constrained, the preference of evapotranspiration (a_{ET}) and the average storage volume ($\overline{S_A}$) were highly correlated and poorly constrained. The level of oxygen-18 in the stream (rather than its variability) helped to constrain the preference of evapotranspiration for the youngest water and thereby also the average subsurface storage. Shorter lived cosmogenic isotopes sodium-22 and sulfur-35 confirmed the shape of the age distribution. Few prior applications of sodium-22 have been published (Kaste et al., 2016) and are mostly limited to lake residence time studies (Sakaguchi et al., 2005). Applications of sulfur-35 are more widespread, and recent studies have demonstrated its use to derive the residence time of managed aquifer recharge (Clark et al., 2016; Urióstegui et al., 2015, 2016) and alpine catchments (Urióstegui et al., 2017) in conjunction with other age tracers. Tritium and oxygen-18 combined are powerful tracers for watersheds with similar characteristics, while sodium-22 and sulfur-35 would be more beneficial if shorter flow paths dominate the stream flow generation.

Further study is warranted into the conservative behavior of the ionic isotopic tracers sodium-22 and sulfur-35. Sodium-22 can be subject to cation exchange in soils with high clay or organic matter content. At Providence Creek, a multi-end-member mixing analysis showed that calcium, magnesium, potassium, chloride, and acid neutralizing capacity behave conservatively, whereas sodium and sulfate did not (Liu et al., 2013). Cation exchange capacity of soils in similar geology at this elevation ranged from 180 meq/kg in the topsoil to 51 meq/kg below 1 m depth and was attributed to organic carbon and low cation exchange capacity clays (van de Ven & Mumford, 2018). Exchangeable sodium sorbed to the cation exchange complex was limited to 0.1 to 0.3 meq/kg, compared to 20–80 meq/kg calcium. The low affinity for sodium suggests limited retardation of sodium transport by cation exchange. Sodium-22 is also expected to trace water conservatively in catchments with relatively thin acidic soils or highly weathered quartz-rich soils (Kaste et al., 2016). Sulfur-35 immobilization (e.g., uptake by vegetation or soil microbial processes) has been discussed in prior studies (Böhlke & Michel, 2009; Michel et al., 2000) and needs to be investigated further. Analysis of the stable sulfur isotopic composition (sulfur-34/sulfur-32) of sulfate in hydrological compartments is promising (Urióstegui et al., 2017).

The use of cosmogenic radioactive isotopes as hydrological tracers relies on an adequate reconstruction of the input history in precipitation. This study relied on a combination of newly collected precipitation samples and prior studies. The applicability and reliability of these tracers greatly improves by a more thorough understanding of the global spatial and temporal variation of these isotopes in precipitation.

4.3. The Role of Evapotranspiration

The level of oxygen-18 in stream flow showed a bias toward winter precipitation, while the variability was minimal. The level of oxygen-18 in the stream was able to constrain the preference of evapotranspiration for younger water, reducing the probable ranges of parameters also for a_{Qmin} and storage volume $\overline{S_A}$. This finding is based on a simplified input reconstruction for oxygen-18 in precipitation (sinusoid function) and snowmelt (reflecting the average oxygen-18 of the entire snowpack), and future studies should perform a more thorough evaluation of the sensitivity to the oxygen-18 input signal. In addition, the fractionating effects of bare soil evaporation on the oxygen-18 input signal were not included. Bare soil evaporation would shift oxygen-18 in storage toward less negative values (away from the winter precipitation signal). If this process was significant and included in the model, the preference of evapotranspiration would need to be stronger to result in the same winter-biased oxygen-18 levels in the stream.

We have not explored the possibility of a storage-dependent storage selection function for water for evapotranspiration. While faster flow paths are activated during wet conditions, justifying a wetness-dependent storage selection function for stream flow, vegetation root structure is generally fixed in space and invariable to wetness. Away from groundwater discharge areas, we argue that vegetation will prefer to access the most easily accessible, often shallowest, and youngest water available, acknowledging that water stored in soils at pressures beyond the wilting point are inaccessible.

Van der Velde et al. (2015) found that the conceptualization of the evapotranspiration flux strongly influences the inferred travel times of stream discharge. Specifically, evapotranspiration removed the younger water from the Marshall Gulch catchment (Arizona, USA), similar to our findings in the Mediterranean Sierra Nevada. Both in the Marshall Gulch catchment and the SS-CZO, this higher preference for young water in evapotranspiration resulted in older water in the stream compared to scenarios with complete mixing or a smaller preference for younger water in evapotranspiration.

While no isotopic data for evapotranspiration was included as an objective for the model, this finding emphasized the importance of studying evapotranspiration and stream flow as a whole within the SAS framework, especially in catchments where evapotranspiration is a significant and important flux in the water balance. Few studies have focused on isotopic evidence in evapotranspiration (Soulsby et al., 2016), yet isotopic evidence has revealed contrasting vegetation water strategies. Isotopic differences between vegetation water, soil water, and stream flow supported the conclusion that vegetation utilizes the first precipitation in the wet season (Brooks et al., 2010). In contrast, the tritium content of apple juice suggested that the mean age of the transpired water was 27 years (Zhang et al., 2017). Considering that evapotranspiration (on average) removes half of the precipitation from the catchment (and in some places nearly all), explicit incorporation of water age is essential to interpret the transit time distribution of the other—better studied—half of the hydrological cycle: stream flow.

4.4. The Role of the Unsaturated Zone

Storage-discharge relationships inherently include unsaturated zone storage changes. Investigations into the derivative of the stream flow rate or the relationship between stream flow and storage have been most successful in places where storage changes are smaller than the annual precipitation by an order of magnitude: that is, in watersheds that drain a significant fraction of each precipitation event before the arrival of the next precipitation event and that return to "base flow" conditions multiple times in a year (Kirchner, 2009). This results in multiple wetting and drying cycles over the course of a year, while Mediterranean catchments often experience a single more intense annual cycle (Pangle et al., 2017). Examining the storage selection for stream flow is intrinsically linked to the relationship between stream flow rate and storage, considering also evapotranspiration (Jepsen, Harmon, & Shi, 2016). Understanding which water leaves a catchment could improve the prediction of how much water leaves a catchment through stream flow.

Storage selection functions have the promise to make the black-box *Q-S* relationship less opaque, more translucent and perhaps even transparent.

The thickness of the unsaturated zone required to store an annual precipitation affects the travel time in the unsaturated zone (Gerber et al., 2018), which is often neglected in dynamic catchment age studies. Vertical flow through the unsaturated zone can delay the arrival of precipitation to saturated zone, challenging concepts developed in "traditional" non-Mediterranean catchments. Details of the storage selection function, related to the very youngest or oldest water, provide insights into the shallowest—often unsaturated—parts of a catchment (M. Kim et al., 2016; Pangle et al., 2017).

A first approximation of unsaturated zone storage in this critical zone is the annual storage change. Unsaturated storage in the top 1 m varies from 100 to 300 mm annually (Oroza et al., 2018). Annual storage changes averaged over the entire watershed are typically on the order of 600 mm. Based on a storage capacity of 200-mm water per meter depth, 3 m of unsaturated zone are required—on average over the entire catchment—to store the annual storage change of 600 mm (Figure S2.3). At the lowest storage conditions, 100 mm of water remain in the top 1 m of the unsaturated zone (Oroza et al., 2018). Extrapolating this residual water content to a 3-m unsaturated zone leaves a residual of at least 300 mm of unsaturated storage. This first-order estimate is the equivalent of 10% of the total storage parameter and appears to be small compared to the total average subsurface storage of 3 m in the Providence Creek watershed. Including the water balance data, total subsurface storage in P301 varied from a low of 2.7 m during the drought to a high of nearly 4.0 m during peak storage in wet years like 2011.

Numerical model evaluations of the critical zone (e.g., Jepsen, Harmon, Meadows, & Hunsaker, 2016) can elucidate on the age accumulation in the unsaturated zone. Prior numerical evaluations of age distributions in mountainous catchments at high resolution (Engdahl & Maxwell, 2015) or at the continental scale at coarser resolution (Maxwell et al., 2016) have demonstrated that vadose zone and land surface processes significantly affect both the residence time distributions and their spectra. (Kollet & Maxwell, 2008).

4.5. Hydrochronological Constraints on Storage and Weathering

The storage selection behavior contains information about the architecture of the catchment in a number of ways. The active storage parameter $\overline{S_A}$ was constrained to 3 m of water. The storage potential of the SS-CZO was previously estimated at 3 m (Holbrook et al., 2014). This geophysical estimate of storage was limited to a transect across a forested slope and a swampy meadow. A weathering zone of 10 to 35 m retrieved from seismic refraction and resistivity imaging was combined with physical properties from hand augering to estimate water storage capacity. While neither estimate is precise, active storage provides significant interannual carryover which sustains the meadows through droughts. The thickness of the weathered bedrock and the subsurface storage of water is the combined effect of the position of the Critical Zone Observatory (on the edge of a tread in the stepped terrain of the Southern Sierras; Jessup et al., 2011; Figure 1) and the bedrock-controlled landscape evolution (Hahm et al., 2014). Hydrochronological constraints on subsurface storage provide landscape-integrated metrics of the critical zone architecture.

The integrated storage in a catchment can help constrain weathering rates and depth to unweathered bedrock for the catchment as a whole. The oldest water discharging the catchment may seem old on the time scale of most hydrological processes; on the geological time scale of weathering and landscape evolution, it is not. The preference for the oldest water we found at the SS-CZO has implications also for weathering mechanisms. While this result does not rule out the presence of stagnant water in bedrock fractures (because that would not be observed in stream flow), it does suggest that the architecture of the catchment facilitates the removal of the oldest water from permeable fractured bedrock. Discharging the oldest water from a catchment inherently means replacing that oldest water that is stored in deeper parts of the subsurface (Rempe & Dietrich, 2014). The replacement rate has implications for the delivery of weathering agents (O_2, CO_2) to weathering fronts (Ferrier et al., 2016; Riebe et al., 2017). The investigation of ages in stream flow gives a strong indication of the importance of water flow for weathering potential.

5. Conclusions

We have presented the first study to combine the cosmogenic radioactive isotopes tritium, sodium-22, and sulfur-35 and the stable isotope oxygen-18 to constrain age-ranked storage selection functions. The hydrochronology of a subalpine stream was characterized by transit time distributions that vary in time, depending on stream flow rate, as a result of time-variable storage selection. We found that the hydrological state of the catchment controls how the critical zone selects water from storage for stream flow. We found that the critical zone of the P301 subcatchment of Providence Creek contains on average 3 m of water in storage. Stream discharge reflects a strong preference for the oldest water in storage during dry conditions, which changes to a slight preference for younger water during wet conditions. A preference of evapotranspiration to extract younger water from storages was constrained by the levels of oxygen-18 in stream flow and needs to be further constrained by isotopic or other investigations of evaporation and transpiration. Tritium and oxygen-18 combined are powerful tracers for watersheds with similar characteristics. Sodium-22 and sulfur-35 would be more beneficial if shorter flow paths dominate the stream flow generation, but more research is needed to understand their reactivity within the critical zone.

The hydrochronology of the critical zone is here defined as the sequential contribution of past precipitations events to the water balance as a consequence of the sequential order in which past precipitation and discharge events occurred. As such, it fits neatly within the framework of the age-ranked storage selection. Unraveling the hydrochronology of the critical zone using cosmogenic isotopes increases our understanding of water storage dynamics and constrains the subsurface storage, weathering, and erosion processes in relation to catchment position and landscape evolution.

Acknowledgments
We thank Mike Sharp for tritium sample analyses; the U.S. Forest Service Pacific Southwest Research Station, in particular Carolyn Hunsaker, for water balance data; Erik Oerter for insightful discussions on evapotranspiration; and Christie Egnatuk and Keenan Thomas for low-level gamma counting expertise. All new measurements necessary to evaluate, replicate, and build upon this research is presented in tables or in the supporting information. Precipitation, snow depth, stream flow, and evapotranspiration data can be obtained from the Southern Sierra Critical Zone Observatory website (http://criticalzone.org/sierra/data/datasets/). Prepared by LLNL under Contract DE-AC52-07NA27344, with funding from Laboratory Directed Research and Development project 15-ERD-042 (LLNL-JRNL-739758). The authors declare no conflict of interest.

References

Anderson, S. P., Bales, R. C., & Duffy, C. J. (2008). Critical zone observatories: Building a network to advance interdisciplinary study of Earth surface processes. *Mineralogical Magazine*, *72*(1), 7–10. https://doi.org/10.1180/minmag.2008.072.1.7

Bales, R. C., White, T., Brantley, S., Banwart, S., Chorover, J., Dietrich, W., et al. (2017). The role of critical zone observatories in critical zone science, Edited.

Benettin, P., & Bertuzzo, E. (2018). Tran-SAS v1.0: A numerical model to compute catchment-scale hydrologic transport using StorAge selection functions. *Geoscientific Model Development*, *11*(4), 1627–1639. https://doi.org/10.5194/gmd-11-1627-2018

Benettin, P., Kirchner, J. W., Rinaldo, A., & Botter, G. (2015). Modeling chloride transport using travel time distributions at Plynlimon, Wales. *Water Resources Research*, *51*, 3259–3276. https://doi.org/10.1002/2014WR016600

Benettin, P., Soulsby, C., Birkel, C., Tetzlaff, D., Botter, G., & Rinaldo, A. (2017). Using SAS functions and high-resolution isotope data to unravel travel time distributions in headwater catchments. *Water Resources Research*, *53*, 1864–1878. https://doi.org/10.1002/2016WR020117

Böhlke, J. K., & Michel, R. L. (2009). Contrasting residence times and fluxes of water and sulfate in two small forested watersheds in Virginia, USA. *Science of the Total Environment*, *407*(14), 4363–4377. https://doi.org/10.1016/j.scitotenv.2009.02.007

Botter, G., Bertuzzo, E., & Rinaldo, A. (2011). Catchment residence and travel time distributions: The master equation. *Geophysical Research Letters*, *38*, L11403. https://doi.org/10.1029/2011GL047666

Brooks, R. J., Barnard, H. R., Coulombe, R., & McDonnell, J. J. (2010). Ecohydrologic separation of water between trees and streams in a Mediterranean climate. *Nature Geoscience*, *3*(2), 100–104. https://doi.org/10.1038/ngeo722

Cartwright, I., & Morgenstern, U. (2018). Using tritium and other geochemical tracers to address the “old water paradox” in headwater catchments. *Journal of Hydrology*, *563*, 13–21. https://doi.org/10.1016/j.jhydrol.2018.05.060

Clark, J., Urióstegui, S., Bibby, R., Esser, B., & Tredoux, G. (2016). Quantifying apparent groundwater ages near managed aquifer recharge operations using radio-sulfur (^{35}S) as an intrinsic tracer. *Water*, *8*(11), 474. https://doi.org/10.3390/w8110474

Druhan, J. L., Fernandez, N., Wang, J., Dietrich, W. E., & Rempe, D. (2017). Seasonal shifts in the solute ion ratios of vadose zone rock moisture from the Eel River Critical Zone Observatory. *Acta Geochimica*, *36*(3), 385–388. https://doi.org/10.1007/s11631-017-0169-z

Ducros, L., Eyrolle, F., Vedova, C. D., Charmasson, S., Leblanc, M., Mayer, A., et al. (2018). Tritium in river waters from French Mediterranean catchments: Background levels and variability. *Science of the Total Environment*, *612*(Supplement C), 672–682. https://doi.org/10.1016/j.scitotenv.2017.08.026

Duvert, C., Stewart, M. K., Cendón, D. I., & Raiber, M. (2016). Time series of tritium, stable isotopes and chloride reveal short-term variations in groundwater contribution to a stream. *Hydrology and Earth System Sciences*, *20*(1), 257–277. https://doi.org/10.5194/hess-20-257-2016

Engdahl, N. B., & Maxwell, R. M. (2015). Quantifying changes in age distributions and the hydrologic balance of a high-mountain watershed from climate induced variations in recharge. *Journal of Hydrology*, *522*, 152–162. https://doi.org/10.1016/j.jhydrol.2014.12.032

Fatichi, S., Pappas, C., & Ivanov, V. Y. (2015). Modeling plant–water interactions: An ecohydrological overview from the cell to the global scale. *Wiley Interdisciplinary Reviews Water*, *3*(3), 327–368.

Ferrier, K. L., Riebe, C. S., & Jesse Hahm, W. (2016). Testing for supply-limited and kinetic-limited chemical erosion in field measurements of regolith production and chemical depletion. *Geochemistry, Geophysics, Geosystems*, *17*, 2270–2285. https://doi.org/10.1002/2016GC006273

Gerber, C., Purtschert, R., Hunkeler, D., Hug, R., & Sültenfuss, J. (2018). Using environmental tracers to determine the relative importance of travel times in the unsaturated and saturated zones for the delay of nitrate reduction measures. *Journal of Hydrology*, *561*, 250–266. https://doi.org/10.1016/j.jhydrol.2018.03.043

Goulden, M. L., Anderson, R. G., Bales, R. C., Kelly, A. E., Meadows, M., & Winston, G. C. (2012). Evapotranspiration along an elevation gradient in California's Sierra Nevada. *Journal of Geophysical Research*, *117*, G03028. https://doi.org/10.1029/2012JG002027

Goulden, M. L., & Bales, R. C. (2014). Mountain runoff vulnerability to increased evapotranspiration with vegetation expansion. *Proceedings of the National Academy of Sciences of the United States of America*, *111*(39), 14,071–14,075. https://doi.org/10.1073/pnas.1319316111

Grant, G. E., & Dietrich, W. E. (2017). The frontier beneath our feet. *Water Resources Research*, *53*, 2605–2609. https://doi.org/10.1002/2017WR020835

Hahm, W. J., Riebe, C. S., Lukens, C. E., & Araki, S. (2014). Bedrock composition regulates mountain ecosystems and landscape evolution. *Proceedings of the National Academy of Sciences*, *111*(9), 3338–3343. https://doi.org/10.1073/pnas.1315667111

Harman, C. J. (2015). Time-variable transit time distributions and transport: Theory and application to storage-dependent transport of chloride in a watershed. *Water Resources Research*, *51*, 1–30. https://doi.org/10.1002/2014WR015707

Harms, P. A., Visser, A., Moran, J. E., & Esser, B. K. (2016). Distribution of tritium in precipitation and surface water in California. *Journal of Hydrology*, *534*, 63–72. https://doi.org/10.1016/j.jhydrol.2015.12.046

He, M., Russo, M., & Anderson, M. (2017). Hydroclimatic characteristics of the 2012–2015 California drought from an operational perspective. *Climate*, *5*(1), 5. https://doi.org/10.3390/cli5010005

Hofmann, H., Cartwright, I., & Morgenstern, U. (2018). Estimating retention potential of headwater catchment using tritium time series. *Journal of Hydrology*, *561*, 557–572. https://doi.org/10.1016/j.jhydrol.2018.04.030

Holbrook, W. S., Riebe, C. S., Elwaseif, M., L. Hayes, J., Basler-Reeder, K., L. Harry, D., et al. (2014). Geophysical constraints on deep weathering and water storage potential in the Southern Sierra Critical Zone Observatory. *Earth Surface Processes and Landforms*, *39*(3), 366–380. https://doi.org/10.1002/esp.3502

Jepsen, S. M., Harmon, T. C., Meadows, M. W., & Hunsaker, C. T. (2016). Hydrogeologic influence on changes in snowmelt runoff with climate warming: Numerical experiments on a mid-elevation catchment in the Sierra Nevada, USA. *Journal of Hydrology*, *533*, 332–342. https://doi.org/10.1016/j.jhydrol.2015.12.010

Jepsen, S. M., Harmon, T. C., & Shi, Y. (2016). Watershed model calibration to the base flow recession curve with and without evapotranspiration effects. *Water Resources Research*, *52*, 2919–2933. https://doi.org/10.1002/2015WR017827

Jessup, B. S., Jesse Hahm, W., Miller, S. N., Kirchner, J. W., & Riebe, C. S. (2011). Landscape response to tipping points in granite weathering: The case of stepped topography in the Southern Sierra Critical Zone Observatory. *Applied Geochemistry*, *26*(Supplement), S48–S50. https://doi.org/10.1016/j.apgeochem.2011.03.026

Jones, J. P., Sudicky, E. A., Brookfield, A. E., & Park, Y. J. (2006). An assessment of the tracer-based approach to quantifying groundwater contributions to streamflow. *Water Resources Research*, *42*, W02407. https://doi.org/10.1029/2005WR004130

Kaste, J. M., Lauer, N. E., Spaetzel, A. B., & Goydan, C. (2016). Cosmogenic ^{22}Na as a steady-state tracer of solute transport and water age in first-order catchments. *Earth and Planetary Science Letters*, *456*, 78–86. https://doi.org/10.1016/j.epsl.2016.10.002

Kim, H., Dietrich, W. E., Thurnhoffer, B. M., Bishop, J. K. B., & Fung, I. Y. (2017). Controls on solute concentration-discharge relationships revealed by simultaneous hydrochemistry observations of hillslope runoff and stream flow: The importance of critical zone structure. *Water Resources Research*, *53*, 1424–1443. https://doi.org/10.1002/2016WR019722

Kim, M., Pangle, L. A., Cardoso, C., Lora, M., Volkmann, T. H. M., Wang, Y., et al. (2016). Transit time distributions and StorAge selection functions in a sloping soil lysimeter with time-varying flow paths: Direct observation of internal and external transport variability. *Water Resources Research*, *52*, 7105–7129. https://doi.org/10.1002/2016WR018620

Kirchner, J. W. (2003). A double paradox in catchment hydrology and geochemistry. *Hydrological Processes*, *17*(4), 871–874. https://doi.org/10.1002/hyp.5108

Kirchner, J. W. (2009). Catchments as simple dynamical systems: Catchment characterization, rainfall-runoff modeling, and doing hydrology backward. *Water Resources Research*, *45*, W02429. https://doi.org/10.1029/2008WR006912

Kollet, S. J., & Maxwell, R. M. (2008). Demonstrating fractal scaling of baseflow residence time distributions using a fully-coupled groundwater and land surface model. *Geophysical Research Letters*, *35*, L07402. https://doi.org/10.1029/2008GL033215

Liu, F., Hunsaker, C., & Bales, R. C. (2013). Controls of streamflow generation in small catchments across the snow–rain transition in the southern Sierra Nevada, California. *Hydrological Processes*, *27*(14), 1959–1972. https://doi.org/10.1002/hyp.9304

Martinec, J. (1975). Subsurface flow from snowmelt traced by tritium. *Water Resources Research*, *11*(3), 496–498. https://doi.org/10.1029/WR011i003p00496

Maxwell, R. M., Condon, L. E., Kollet, S. J., Maher, K., Haggerty, R., & Forrester, M. M. (2016). The imprint of climate and geology on the residence times of groundwater. *Geophysical Research Letters*, *43*, 701–708. https://doi.org/10.1002/2015GL066916

McDonnell, J. J. (2017). Beyond the water balance. *Nature Geoscience*, *10*(6), 396–396. https://doi.org/10.1038/ngeo2964

McGuire, K. J., & McDonnell, J. J. (2006). A review and evaluation of catchment transit time modeling. *Journal of Hydrology*, *330*(3–4), 543–563. https://doi.org/10.1016/j.jhydrol.2006.04.020

Michel, R. L., Campbell, D., Clow, D., & Turk, J. T. (2000). Timescales for migration of atmospherically derived sulphate through an alpine/subalpine watershed, Loch Vale Colorado. *Water Resources Research*, *36*(1), 27–36. https://doi.org/10.1029/1999WR900276

Morgenstern, U., Stewart, M. K., & Stenger, R. (2010). Dating of streamwater using tritium in a post nuclear bomb pulse world: Continuous variation of mean transit time with streamflow. *Hydrology and Earth System Sciences*, *14*(11), 2289–2301. https://doi.org/10.5194/hess-14-2289-2010

Oroza, C. A., Bales, R. C., Stacy, E. M., Zheng, Z., & Glaser, S. D. (2018). Long-term variability of soil moisture in the Southern Sierra: Measurement and prediction. *Vadose Zone Journal*, *17*(1). https://doi.org/10.2136/vzj2017.10.0178

Pangle, L. A., Kim, M., Cardoso, C., Lora, M., Meira Neto, A. A., Volkmann, T. H. M., et al. (2017). The mechanistic basis for storage-dependent age distributions of water discharged from an experimental hillslope. *Water Resources Research*, *53*, 2733–2754. https://doi.org/10.1002/2016WR019901

Queloz, P., Carraro, L., Benettin, P., Botter, G., Rinaldo, A., & Bertuzzo, E. (2015). Transport of fluorobenzoate tracers in a vegetated hydrologic control volume: 2. Theoretical inferences and modeling. *Water Resources Research*, *51*, 2793–2806. https://doi.org/10.1002/2014WR016508

Rempe, D. M., & Dietrich, W. E. (2014). A bottom-up control on fresh-bedrock topography under landscapes. *Proceedings of the National Academy of Sciences of the United States of America*, *111*(18), 6576–6581. https://doi.org/10.1073/pnas.1404763111

Riebe, C. S., Hahm, W. J., & Brantley, S. L. (2017). Controls on deep critical zone architecture: A historical review and four testable hypotheses. *Earth Surface Processes and Landforms*, *42*(1), 128–156. https://doi.org/10.1002/esp.4052

Rinaldo, A., Benettin, P., Harman, C. J., Hrachowitz, M., McGuire, K. J., Van der Velde, Y., et al. (2015). Storage selection functions: A coherent framework for quantifying how catchments store and release water and solutes. *Water Resources Research*, *51*, 4840–4847. https://doi.org/10.1002/2015WR017273

Safeeq, M., & Hunsaker, C. T. (2016). Characterizing runoff and water yield for headwater catchments in the southern Sierra Nevada. *JAWRA Journal of the American Water Resources Association*, *52*(6), 1327–1346. https://doi.org/10.1111/1752-1688.12457

Sakaguchi, A., Ohtsuka, Y., Yokota, K. I., Sasaki, K., Komura, K., & Yamamoto, M. (2005). Cosmogenic radionuclide ^{22}Na in the Lake Biwa system (Japan): Residence time, transport and application to the hydrology. *Earth and Planetary Science Letters*, *231*(3–4), 307–316. https://doi.org/10.1016/j.epsl.2004.12.023

Seibert, J., Grabs, T., Köhler, S., Laudon, H., Winterdahl, M., & Bishop, K. (2009). Linking soil- and stream-water chemistry based on a riparian flow-concentration integration model. *Hydrology and Earth System Sciences*, *13*(12), 2287–2297. https://doi.org/10.5194/hess-13-2287-2009

Soulsby, C., Birkel, C., & Tetzlaff, D. (2016). Characterizing the age distribution of catchment evaporative losses. *Hydrological Processes*, *30*(8), 1308–1312. https://doi.org/10.1002/hyp.10751

St. Clair, J., Moon, S., Holbrook, W. S., Perron, J. T., Riebe, C. S., Martel, S. J., et al. (2015). Geophysical imaging reveals topographic stress control of bedrock weathering. *Science*, *350*(6260), 534–538. https://doi.org/10.1126/science.aab2210

Urióstegui, S. H., Bibby, R. K., Esser, B. K., & Clark, J. F. (2015). Analytical method for measuring cosmogenic ^{35}S in natural waters. *Analytical Chemistry*, *87*(12), 6064–6070. https://doi.org/10.1021/acs.analchem.5b00584

Urióstegui, S. H., Bibby, R. K., Esser, B. K., & Clark, J. F. (2016). Quantifying groundwater travel time near managed recharge operations using ^{35}S as an intrinsic tracer. *Journal of Hydrology*, *543*, 145–154. https://doi.org/10.1016/j.jhydrol.2016.04.036

Urióstegui, S. H., Bibby, R. K., Esser, B. K., & Clark, J. F. (2017). Quantifying annual groundwater recharge and storage in the Central Sierra Nevada using naturally occurring ^{35}S. *Hydrological Processes*, *31*(6), 1382–1397. https://doi.org/10.1002/hyp.11112

Van de Ven, C. J. C., & Mumford, K. G. (2018). Visualization of gas dissolution following upward gas migration in porous media: Technique and implications for stray gas. *Advances in Water Resources*, *115*, 33–43.

Van der Velde, Y., de Rooij, G. H., Rozemeijer, J. C., van Geer, F. C., & Broers, H. P. (2010). Nitrate response of a lowland catchment: On the relation between stream concentration and travel time distribution dynamics. *Water Resources Research*, *46*, W11534. https://doi.org/10.1029/2010WR009105

Van der Velde, Y., Heidbüchel, I., Lyon, S. W., Nyberg, L., Rodhe, A., Bishop, K., & Troch, P. A. (2015). Consequences of mixing assumptions for time-variable travel time distributions. *Hydrological Processes*, *29*(16), 3460–3474. https://doi.org/10.1002/hyp.10372

Van der Velde, Y., Torfs, P. J. J. F., van der Zee, S. E. A. T. M., & Uijlenhoet, R. (2012). Quantifying catchment-scale mixing and its effect on time-varying travel time distributions. *Water Resources Research*, *48*, W06536. https://doi.org/10.1029/2011WR011310

Visser, A., Thaw, M., & Esser, B. (2018). Analysis of air mass trajectories to explain observed variability of tritium in precipitation at the Southern Sierra Critical Zone Observatory, California, USA. *Journal of Environmental Radioactivity*, *181*, 42–51. https://doi.org/10.1016/j.jenvrad.2017.10.008

Zhang, Z. Q., Evaristo, J., Li, Z., Si, B. C., & McDonnell, J. J. (2017). Tritium analysis shows apple trees may be transpiring water several decades old. *Hydrological Processes*, *31*(5), 1196–1201. https://doi.org/10.1002/hyp.11108